NEW UNDERSTANDING OF MULTI-SCALE PEDESTAL TURBULENCE, TRANSPORT, AND GRADIENT BEHAVIOR DURING TYPE-I ELMS ON THE DIII-D TOKAMAK

K. BARADA, T. L. RHODES, L. ZENG, J. CHEN, G. WANG
Department of Physics and Astronomy, UCLA
Los Angeles, USA
Email: kshitish@ucla.edu

S. R. HASKEY, A. DIALLO, F. LAGGNER
Princeton Plasma Physics Laboratory
Princeton, USA

S. BANERJEE
Department of Physics, College of William and Mary
Williamsburg, USA

R. GROEBNER
General Atomics
San Diego, USA

Z. YAN
University of Wisconsin-Madison
Madison, USA

Abstract

New observations of pedestal localized turbulence in the inter-ELM period of DIII-D show that ITG-scale density fluctuation (ñ) increases right after ELM crash and is quickly suppressed by an increase in local ExB shear. This excitation and subsequent suppression of ITG-scale ñ can explain the previously reported anomalous ion heat flux, Qi during the ELM that then becomes neo-classical (E. Viezzer et al, 2017 Nucl. Fusion 57 022020) on a longer timescale leading up to next ELM. Shorter wavelength TEM-scale ñ starts to increase at a critical pedestal temperature gradient ($\nabla T_{e,ped}$) and saturates as both local ExB shear, T_i^{C6+}/T_e ratio, and $\nabla T_{e,ped}$ increase and saturate. This TEM-scale ñ, which has potential to cause electron heat transport, is consistent with driving an anomalous electron heat flux Qe (Q_e estimated between ELMs using experimental profiles and power balance). ITG and TEM-scale ñ amplitude variations with background T_i/T_e and $\nabla n_{e,\,ped}$ are found to be consistent with theoretical predictions of these measured ñ being ITG and TEM instabilities respectively. These new and unique observations on the nature of turbulence and their contributions to electron and ion heat fluxes at different ELM periods (i.e., collapse, recovery, and saturation phases of pedestal gradients) can significantly test and improve our predictive capabilities leading to better optimization of fusion performance in ITER and other future fusion devices.

1. INTRODUCTION

Improved confinement due to suppression of edge turbulence by ExB shear leads to the L-H transition and formation of a narrow steep gradient region called the pedestal in the plasma edge. ITER [1] will operate in H-mode with power levels close to the L-H threshold where existing experiments display large and low frequency type-I edge localized modes (ELMs) that periodically perturb the pedestal gradients. The ELMs can also deposit large amounts particle and heat flux on to the divertor and other plasma facing components leading to their untimely degradation. Based on extrapolations, the largest ELMs [ELM energy loss > 1MJ [2]] cannot be tolerated regularly in ITER. Lack of understanding of all of the processes involved in pedestal evolution leads to considerable uncertainty with predictions of inter-ELM energy losses [3]. Although the height, width, and the gradients are limited ultimately by the coupled peeling-ballooning (PB) MHD modes, understanding of how the pedestal approaches this limit and different transport mechanisms responsible in the inter-ELM period will help us predict the height and width of the pedestal. After each ELM event, the pedestal gradients decrease, recover, and then can stay nearly saturated and close to the PB-unstable boundary for a significant portion of the inter-ELM period [4]. These observations from many tokamaks indicate turbulent transport might play a role in maintaining the saturated gradients. It has been proposed [5] that kinetic ballooning mode (KBM) drives sufficient thermal and particle flux to keep the pressure gradient nearly clamped until the PB modes excite an ELM event. KBM being an MHD mode is expected [3] to equally drive both electron and ion heat fluxes whereas ion thermal

fluxes estimated from experimental power balance suggest ion heat flux being close to neoclassical levels [6] in the saturated phase of inter-ELM period. Recent calculations [7, 8] using measured main ion density and temperature in DIII-D H-mode plasmas show that at high pedestal collisionality, the ion heat flux is approximately a factor of two higher than neoclassical levels with this difference increasing as the collisionality is lowered. These ion heat flux estimations indicate a role of transport from ion scale turbulent fluctuations at different collisionalities. Electron heat flux has been estimated to be always anomalous and this anomalous heat flux can limit the electron temperature pedestal gradient to further increase. Using gyrokinetic simulations in the pedestal, microtearing (MTM) and electron temperature gradient (ETG) modes are proposed in the "fingerprint" model [3] to drive significant electron heat flux in the pedestal. MTM-like low-k fluctuations, recently reported [9, 10] from measurements of magnetic and density fluctuations in the inter-ELM period by radial interferometer polarimeter (RIP) and beam emission spectroscopy (BES) show a correlation of MTM-like fluctuation amplitude with $\nabla T_{e,ped}$. Similar correlation has not been observed in the discharges reported here and identification of the magnetic fluctuations observed by RIP and external mirnov coils are inconclusive. It is to be noted that the discharges described in this manuscript are very different from that reported in [9, 10]. ETG modes are recently [11] shown to contribute to the electron thermal flux although ETG scale fluctuations are not measured in the discharges mentioned in this paper. The EPED model [5] successfully (within $\pm 15\%$ uncertainty) predicts the pedestal width just before ELM event for a given pedestal height using the PB and KBM constraints on height and width respectively. However, the role of ion temperature gradient (ITG) and trapped electron mode (TEM) scale turbulence has not been extensively discussed so far or have been hypothesized to be ExB shear suppressed. If present these modes could drive significant ion and electron thermal, particle and impurity fluxes. However, there are pedestal locations, namely the foot, top, and steep gradient region (close to E_r well) of the pedestal where the measured ExB shear is much smaller than compared to the outer and inner shear layers of the radial electric field profile, and these regions can accommodate electrostatic fluctuations [12] if the drive for turbulence therein is strong enough. In this manuscript, role of observed ITG and TEM-scale turbulence are studied in a type-I ELMing discharge by correlating their amplitude evolutions with various pedestal parameters and inferred electron and ion heat fluxes. The very fact that these turbulent fluctuations are measured indicates these are not completely shear suppressed in the pedestal in different inter-ELM phases of more than 50 similar shots analysed.

Section 2 describes briefly the experimental conditions and parameters along with the major diagnostics used for fluctuation and profile measurements. Section 3 describes the ELM-synchronized pedestal gradient behaviour in the inter-ELM period followed by description of ITG and TEM-scale ñ evolution in the inter-ELM period. A summary of the results and future research directions are given in section 4.

2. OVERVIEW OF EXPERIMENTAL CONDITIONS AND DIAGNOSTICS USED

Experiments are performed in ITER similar shape (ISS) lower single null plasmas (Figure 1a) with plasma current of ~1 MA, toroidal magnetic field of ~2.1 T, injected neutral beam power of ~ 2.3 MW and chord averaged electron density (figure 1d) of 5x1019/m3. The first ELM appears at ~1292 ms and multiple low frequency ELMs are observed in the divertor Dα signal (Figure 1b) with average inter-ELM period of ~78 ms and frequency ~13 Hz. The pedestal electron density (Figure 1c), temperature (Figure 1d), and pressure (Figure 1e) vary with each ELM event. The height and width calculated from the tanh fitting [13] of the Thomson scattering diagnostics measured electron pedestal profiles are used to obtain the ELM synchronized pedestal gradients of electron density, temperature, and pressure. Figure 1f shows a density profile fitted to Thomson scattering measured density wherein modified tanh fitting is applied to the edge and the height and width of the pedestal are also shown.

Density fluctuations and associated Doppler shifts are measured using Doppler backscattering (DBS) diagnostics [14]. DBS measures spatially, temporally, and wave number resolved ñ amplitude along with the ñ lab frame perpendicular velocity, $v_\perp$. It has been found that ñ from the vicinity of the cut-off layer dominates the backscattering of the incident wave and the 180º backscattered radiation is collected when the Bragg condition ($k_{\tilde{n}}$=−$2k_i$) for scattering is fulfilled. Here, $k_{\tilde{n}}$ is the density fluctuation wavenumber and k_i is the incident wavenumber at the cut-off location. The backscattered signal is Doppler shifted with respect to incident wave with a Doppler shifted frequency $f_D = k_{\tilde{n}} v_\perp / 2\pi$, where $v_\perp = v_{E\times B} + v_{ph}$ and the intensity of the received signal is proportional to ñ. Here $v_{E\times B}$ is the local ExB velocity and v_{ph} is the turbulence phase velocity. Using three different DBS systems, density fluctuations and their velocities are measured at 20 different radial locations from

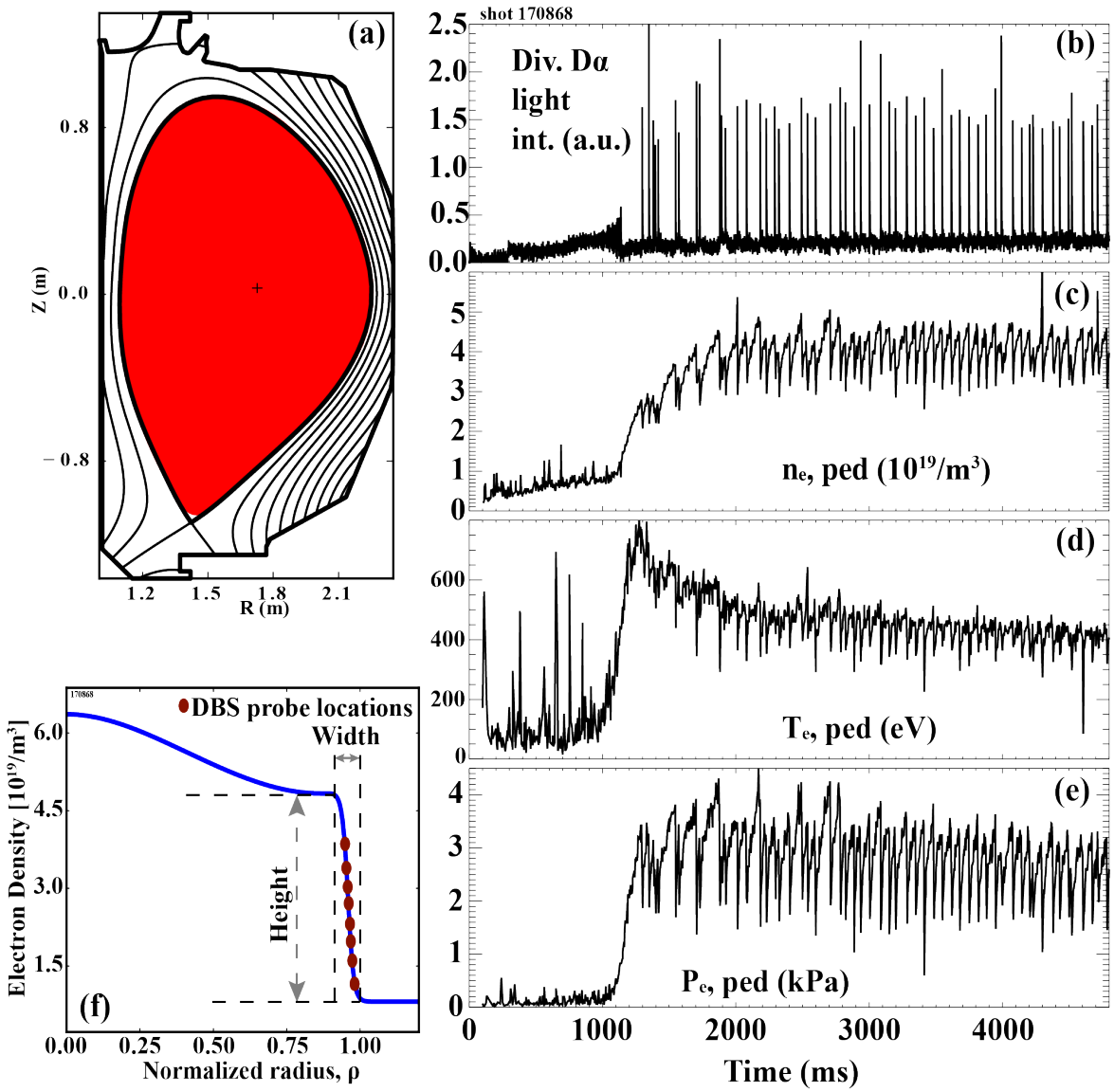

FIG 1. *(a) LSN plasma equilibrium and shape, time variations of important plasma parameters in a type-I ELMing H-mode discharge (b) Divertor Dα light intensity, (c) Pedestal electron temperature, (d) Pedestal electron density, (e) Pedestal electron pressure, and (f) Typical density profile showing height and width of ne pedestal and the eight DBS probed locations are shown as red dots on the density profile.*

the core to the foot of the pedestal. Only the fluctuation measurements in the pedestal will be discussed in this work and these measurement locations are shown as filled circles on the density profile shown in Figure 1f. High time resolution profile reflectometry measured density profiles are used to get DBS scattering locations and probed wavenumbers using GENRAY [15] raytracing. Profile reflectometry is also used to get high time resolution profile density gradients in the pedestal. High and low frequency magnetic fluctuations are measured using Mirnov coils and ion saturation current is measured using floor Langmuir probes located at the outer strike point.

3. INTER-ELM PEDESTAL GRADIENT AND TURBULENCE BEHAVIOR

ELM-synchronized electron pedestal gradients are calculated using the tanh fit Thomson profiles (as discussed in section 2) and are shown in Fig 2. As seen in figure 2a the pedestal electron density gradient ($\nabla n_{e,ped}$), relaxes and then recovers rapidly within 4-5 ms and then evolves slowly for another ~15 ms after which it remains approximately saturated. After the pedestal density gradient's rapid recovery, the pedestal electron temperature gradient ($\nabla T_{e,ped}$, Fig 2b) starts to increase slowly, matching with the

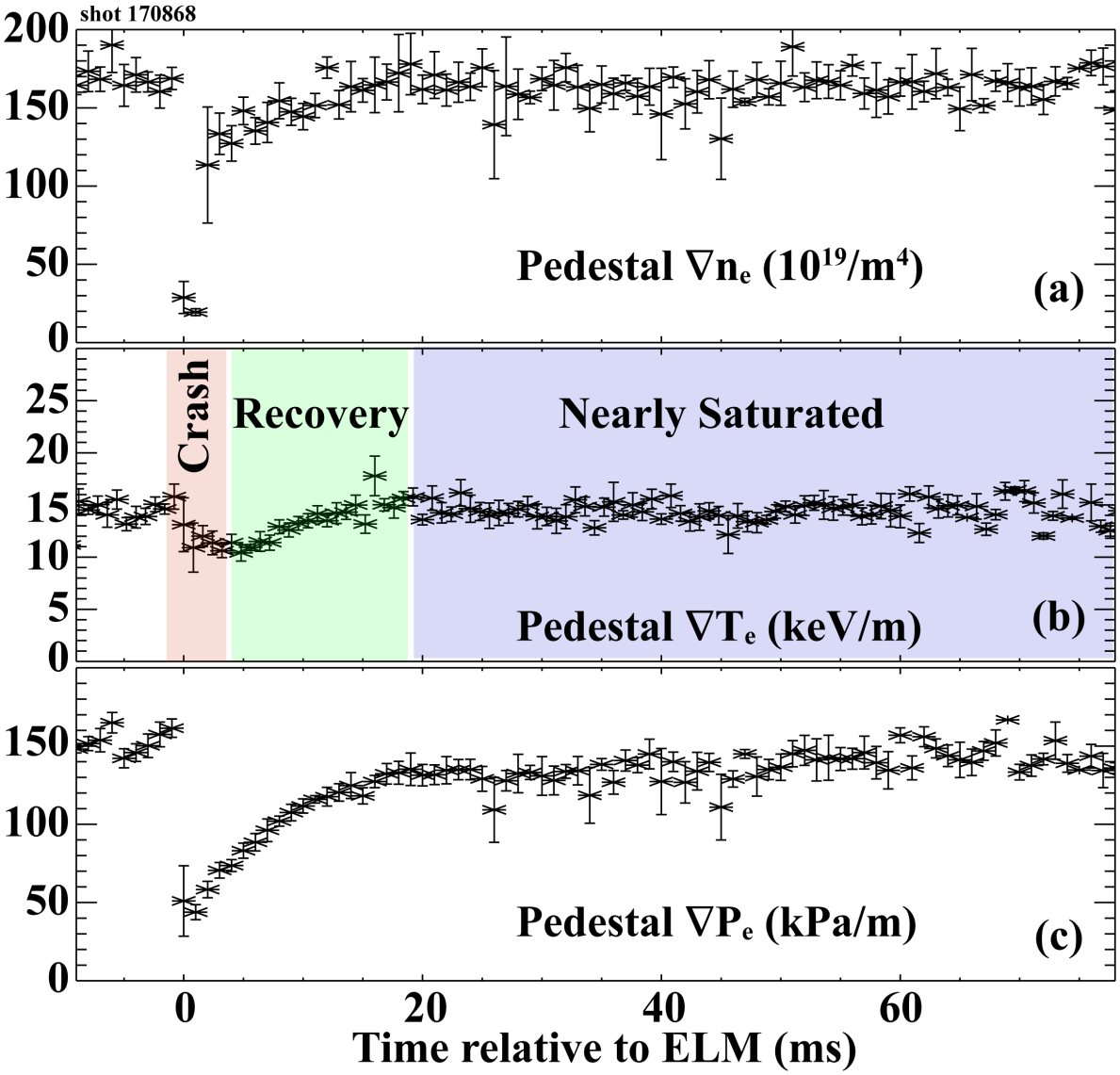

FIG 2. *ELM-synchronized behaviours (a) Pedestal electron density gradient, (b) Pedestal electron temperature gradient (crash, recovery, and nearly saturated phases are shown in shaded colours), (c) Pedestal electron pressure gradient.*

slower recovery timescale of the electron density gradient. After this slower recovery, $\nabla T_{e,ped}$ remains approximately saturated for the rest of inter-ELM period. The electron pedestal pressure gradient ($\nabla P_{e,ped}$, Fig 1c) increases until t~20 ms when electron density and temperature gradients saturate and then very slowly increases for the rest of the inter-ELM period. Similar eelctron pedestal gradient evolution has been reported [16] before in DIII-D. The slow increase in electron pressure gradient is due to the slow increase in pedestal elecctron density (not shown) after t~20 ms from the ELM crash.

The radial range of measurements by the DBS data presented here spans from ρ~0.98 to ρ~0.93 (see Figure 1f) so that the locations close to the separatrix, maximum pressure gradient location and the upper half of the pedestal close to the pedestal top are probed. ñ with $k_\theta \rho_s$~0.3-1.2 are measured which correspond to typical ITG ($0.05 \leq k_\theta \rho_s \leq 0.5$) and TEM ($0.5 \leq k_\theta \rho_s \leq 2$) scales [17]. Here k_θ is the electron density fluctuation wavenumber and ρ_s is the ion Larmor radius estimated using Ti=Te. Section 3.1 describes the ITG-scale ñ and its temporal behaviour and correlations with divertor Dα light intensity and $\nabla n_{e,ped}$. Section 3.2 describes the TEM-scale ñ behaviours and its correlation with various pedestal parameters like T_i/T_e ratio, local ExB shear, and $\nabla T_{e,ped}$.

3.1 ITG-SCALE ñ BEHAVIOR NEAR FOOT OF THE PEDESTAL CLOSE TO THE SEPARATRIX

Figure 3a shows the spectrum of DBS measured ñ intensity with $k_\theta \rho_s$~0.3 (in a similar shot as described in Figure 2) which is well within the ITG-scale. The RMS value of these fluctuation is obtained by integrating the turbulence

intensity over the frequency range of -600 kHz to +300 kHz and its temporal behaviour is shown in Figure 3b. The ITG-scale ñ rms value increases right after the ELM crash (the ELM crash is indicated by the large spike in divertor D_α light intensity in Figure 3c). Within a few ms, the ITG-scale ñ decreases rapidly and continues to decrease at a slower rate until the next ELM. There is a very good correlation between the ITG-scale ñ rms evolution with that of divertor D_α light intensity indicating a potential connection of these ñ fluctuations in particle transport and subsequent recycling in the divertor. Note also that while ITG-scale ñ decreases between ELMs a substantial amplitude remains (Figure 3a, b).

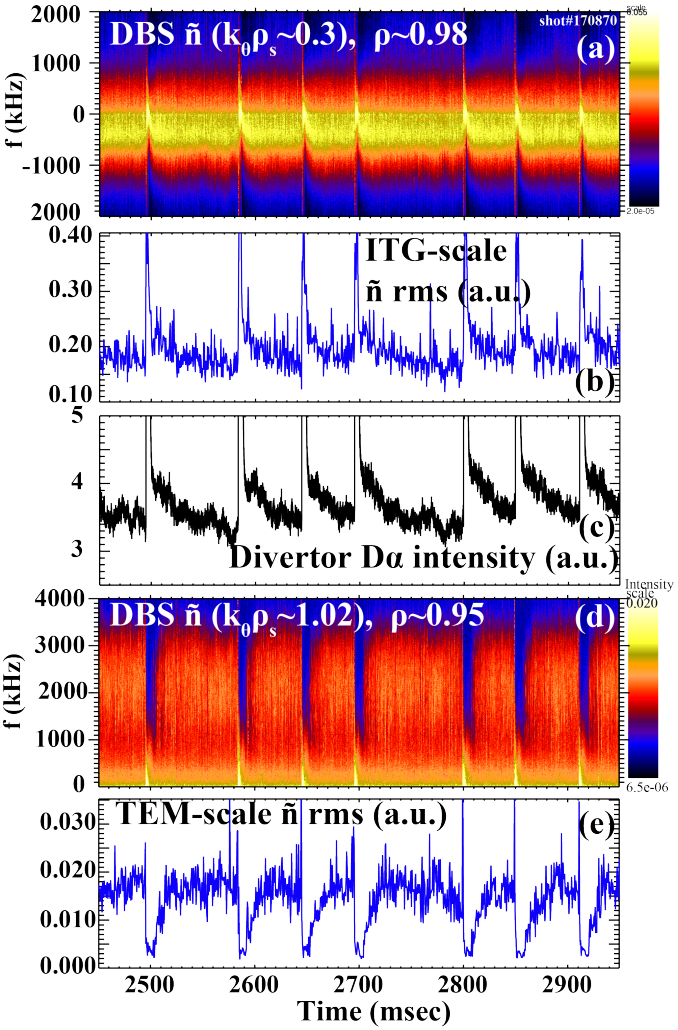

FIG 3. *Temporal variations of (a) Doppler shifted ITG-scale ñ intensity spectrum at ρ~0.98, (b) ñ rms of ITG-scale ñ, (c) Divertor Dα light intensity, (d) Doppler shifted TEM-scale ñ intensity spectrum at ρ~0.95, (e) ñ rms of TEM-scale ñ.*

To gain more understanding of the ITG-scale ñ evolution, ELM-synchronized analysis of important parameters has been done and is correlated with the evolution of local ExB shear (Figure 4c, calculated from high time resolution DBS measurements of local ExB velocity at two adjacent probed locations), divertor D_α light intensity (Figure 4a), and $\nabla n_{e,ped}$ (Figure 4d). As can be seen from Figure 4a and 4b, there is a very good correlation between ELM-synchronized ITG-scale ñ and divertor D_α light intensity. The increase and subsequent reduction of this ITG-scale ñ can be explained by the evolution of the local ExB shear. Just after the ELM crash, when the profiles relax, the local ExB shear decreases and that correlates with an increase in ITG-scale ñ. Within ~1-2 ms the profiles start to recover, the local ExB shear starts to increase, and the ITG-scale ñ is reduced. As the ExB shear slowly increases, the ITG-scale ñ also slowly decreases correlated with a decrease in divertor D_α light intensity. This ITG-scale ñ behaviour is quite consistent with the evolution of ion heat flux estimated from experimental power balance and profiles i.e., right after ELM crash ion heat flux is anomalous (as reported in ASDEX-U tokamak results [6]) and later becomes closer to neoclassical levels. This observed consistency also indicates the role of ITG-scale ñ in particle transport as observed from its correlations with the evolutions of pedestal electron density gradient, which increases and saturates with ITG-scale ñ suppression (Figure 4b and 4d) and divertor D_α light intensity that decreases after ITG-scale ñ suppression.

3.2 TEM-SCALE ñ BEHAVIOR IN THE STEEP GRADIENT REGION

TEM-scale ñ corresponding to $k_\theta \rho_s$~ 0.7-1.2 is measured in the steep gradient region in the radial range of ρ~0.96-0.93. Figure 3d shows DBS measured intensity spectrum of this TEM-scale ñ in the steep gradient for few inter-ELM periods. As can be seen, the ñ intensity and its rms values (Figure 3e) increase ~10 ms after the ELM event and this notable time delay is consistently present in all radial locations described here. GENRAY raytracing calculations using high time resolution profile reflectometry measured density profiles show that the probed locations are not significantly changing in the steep gradient region with most of the changes in electron density

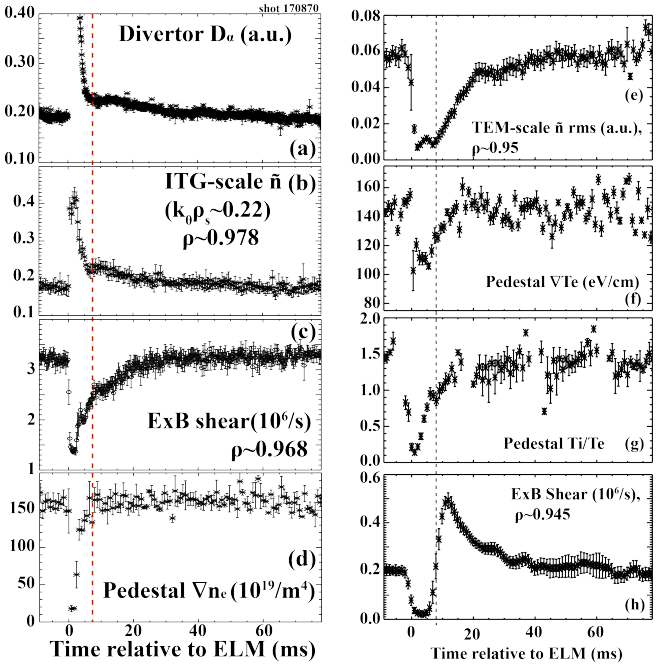

FIG 4. *ELM-synchronized temporal behaviour of (a) Divertor Dα light intensity (b) ITG-scale ñ rms at ρ~0.98, (c) Local ExB shear at ρ~0.97, (d) Pedestal density gradient, (e) TEM-scale ñ rms at ρ~0.95, (f) Pedestal electron temperature gradient, (g) Pedestal T_i/T_e, and (h) Local ExB shear from DBS at ρ~0.945.*

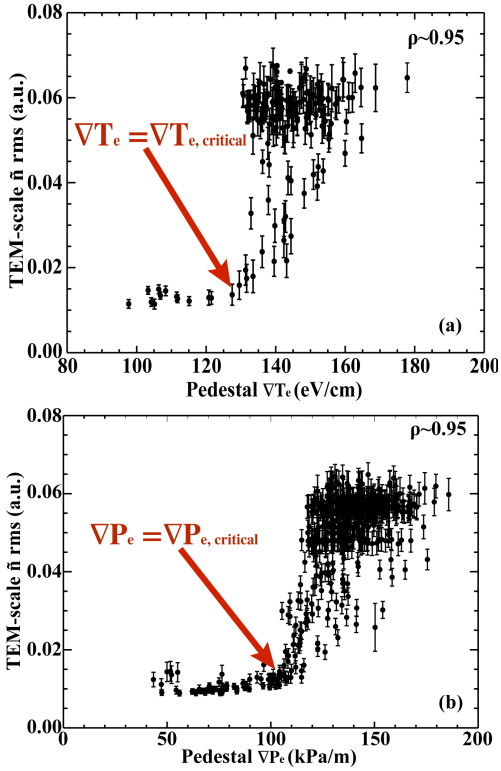

FIG 5. *Variation of ELM-synchronized TEM-scale ñ measured in the steep gradient region with that of pedestal electron (a) temperature and (b) pressure gradient showing critical gradient behavior.*

profile happening at the pedestal top and inward radial locations after ELM event. To understand this sudden increase in TEM-scale ñ, ELM-synchronized analyses are performed and the resultant ñ rms evolution at ρ~0.95 (Figure 4e) is correlated with variations in pedestal $\nabla T_{e,ped}$ (Figure 4f), pedestal T_i/T_e (Figure 4g) at ρ~0.97 (note that first few ms of Ti data might be contaminated by the ELM event), and local ExB shear (Figure 4h) calculated from DBS measured Doppler shifts in the inter-ELM period.

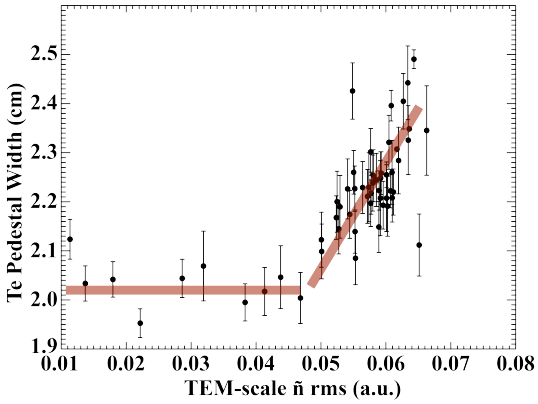

FIG 6. *Variation of ELM-synchronized electron temperature pedestal width with TEM-scale ñ. The red lines are meant as a guide to the eye.*

The ELM-synchronized $\nabla T_{e,ped}$ is plotted against TEM-scale ñ in Figure 5a. As $\nabla T_{e,ped}$ increases, TEM-scale ñ does not increase until ~130 eV/cm where a large increase in the TEM-scale ñ is observed. It is well known that ∇T_e can drive trapped electron modes and the critical ∇T_e required [18] depends on T_i/T_e ratio, background ∇n_e, local ExB shear, and collisionality, etc. These latter parameters are compared in Figure 4. As can be seen, the increase in T_i/T_e (Figure 4g) with a higher background $\nabla n_{e,ped}$ (Figure 4d) correlate with an increasing TEM-scale ñ and are consistent with theoretical predictions of their contributions to lowering the TEM critical ∇T_e. As an increased ∇n_e also contributes to destabilization, the variation of TEM-scale ñ with $\nabla P_{e,ped}$ (Figure 5b) also exhibits a critical gradient behaviour. As the profile gradients increase, the local ExB shear (Figure 4h) also increases but later decreases and remains at a higher value compared to the time right after the ELM crash. This decrease in the ExB shear can be explained by the observation of an increase in the pedestal width with TEM-scale ñ as shown in Figure 6. Later when $\nabla T_{e,ped}$, $\nabla n_{e,ped}$, and Te/Ti saturate, TEM-scale ñ increases very slowly, and correlated with the slow decrease in ExB shear (Figure 4h).

The ratio of T_i/T_e was modified (decreases ~0.5 times everywhere in the pedestal) by additional electron heating using ECH (Figure 7a). This additional heating decreased $\nabla n_{e,ped}$ and increased $\nabla T_{e,ped}$, leaving $\nabla P_{e,ped}$ nearly

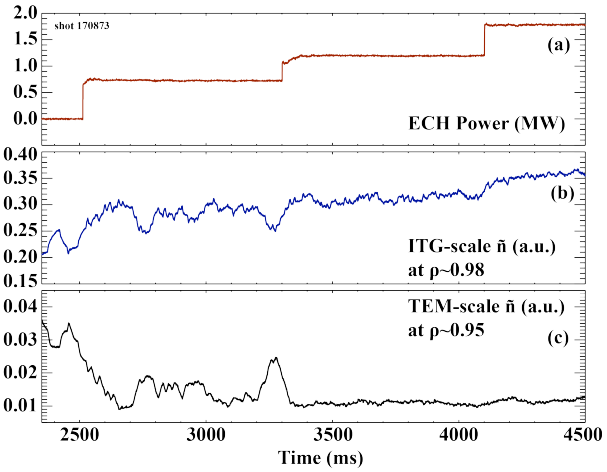

FIG 7. *With additional ECH heating at ρ~0.5, ITG-scale ñ RMS increases and TEM-scale ñ RMS decreases. (a) Time traces of ECH power, (b) ITG-scale ñ RMS, and (c) TEM-scale ñ RMS.*

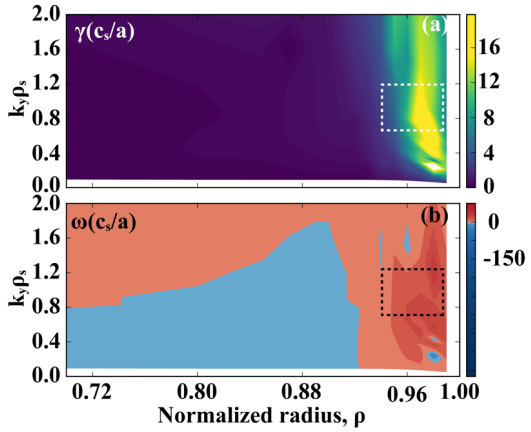

FIG 8. *Linear TGLF simulations showing the contour plot (a) growth rate and (b) mode frequency of the most unstable modes in the $k_y\rho_s$-ρ space. The dashed rectangular areas show the radial and $k_\theta\rho_s$ range of DBS measurements of TEM-scale in the steep gradient during the nearly saturated gradient phase.*

unchanged. In addition, the electron collisionality was reduced by a factor of 4 compared to the purely beam heated discharge. The Te pedestal width does not increase (not shown) unlike for the NBI only discharges as shown in Figure 6. TEM-scale ñ in the steep gradient region decreased by a factor of ~3 (reduced to at or below the noise level, Figure 7c) and ITG-scale ñ (Figure 7b) near the pedestal foot increased ~50%. This is consistent with theoretical predictions [18] of increased ∇T_e threshold for TEM modes and decreased ∇T_i threshold for ITG modes with decreased T_i/T_e and decreased ∇n_e. Initial linear Trapped-Gyro-Landau-Fluid (TGLF) [19] simulations using a plasma kinetic equilibrium and profiles in the nearly saturated phase (70-99% of the inter-ELM period) shows (Figure 8) the most unstable modes propagate in the electron diamagnetic direction in the plasma frame consistent with the DBS measured TEM-scale fluctuations at similar $k_\theta\rho_s$ values in the steep gradient region. Both experimental observations of TEM-scale ñ and TGLF calculations in the steep gradient region are consistent with trapped electron modes. The increased ITG-scale ñ in the case of ECH added discharges is also consistent with recent observations of ion heat flux differing from neoclassical levels at lower collisionalities [7, 8]. Consistent with the remaining ITG-scale ñ reported in Section 3.1 above note the peaked ITG-scale growth rate near $k_\theta\rho_s$~0.2 and ρ~0.98 in Figure 8b.

4. SUMMARY AND DISCUSSIONS

A new understanding of pedestal gradient and heat flux evolutions with pedestal multi-scale fluctuations has been obtained using new multiscale turbulence measurements in DIII-D H-mode plasmas operating close to L-H threshold. Observed ITG-scale fluctuation behaviour can explain the previously observed ion thermal flux variations across an inter-ELM period. Immediately after the profiles relax due to an ELM event, ITG-scale fluctuations increase and are consistent with the anomalous ion heat conductivity previously estimated [6] from experimental power balance and profiles in ASDEX-U tokamak. Once ITG scale fluctuations are supressed by ExB shear, the ITG drive for ion heat flux is expected to be eliminated (not measured here). Thus, the existing observations are consistent with observations in ASDEX-U of the experimental ion heat flux dropping rapidly to neoclassical levels after an ELM event and with measurements in DIII-D of low ion heat flux (Figure 9a) at moderately high collisionality (ν_i^*~0.74). As can also be seen from Figure 9a, the estimated neoclassical heat flux is close to the power balance heat flux only in some radial regions close to the steep gradient region. This difference increases towards the foot of the pedestal and this may be due to the unsuppressed/residual ITG-scale ñ even in the saturated phase as can be seen from Figure 3a, 3b, and Figure 4b. In Figure 9, the experimental thermal fluxes are estimated from power balance calculations using TRANSP [20] code and the neoclassical thermal fluxes are calculated using NEO [21] code. As the pedestal

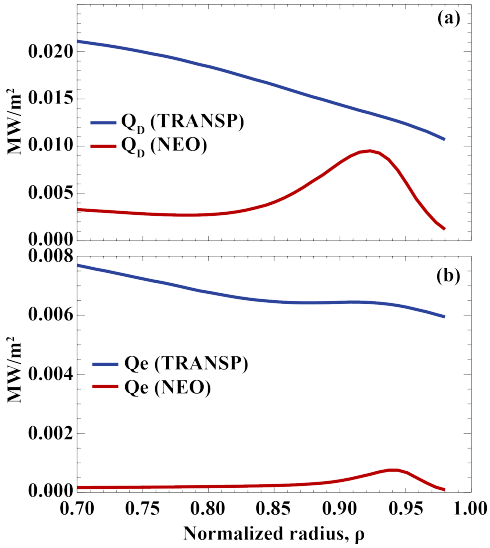

FIG 9. *Comparisons of thermal fluxes estimated from power balance and neoclassical calculations for (a) Main ion and (b) electron in the saturated phase of the inter-ELM period.*

temperature gradient starts to increase, TEM-scale ñ increases accompanied by an increased T_i/T_e and a higher $\nabla n_{e,ped}$ compared to their values right after the ELM-crash. TEM-scale ñ can contribute to the anomalous nature of electron heat flux as observed in both ASDEX-U and in this experiment (Figure 9b) during the saturated phase of the inter-ELM period. It is to be noted that turbulent fluxes from nonlinear gyrokinetic simulations are required to explain the differences between neoclassical and experimental thermal fluxes shown in Figure 9. Adding ECH to beam heated discharges led to suppression of TEM-scale ñ and increase of ITG-scale ñ. These observations are consistent with the opposing effects of decreased T_i/T_e on these fluctuations. Initial TGLF calculations and theoretically expected response of the fluctuations to ECH heating or decreased T_i/T_e are consistent with both ion temperature gradient and trapped electron modes; however, positive identification requires a cautious approach.

ACKNOWLEDGEMENTS

This material is based upon work supported by the U.S. Department of Energy, Office of Science, Office of Fusion Energy Sciences, using the DIII-D National Fusion Facility, a DOE Office of Science user facility, under Award(s) DE-FG02-08ER54984, DE-AC02-09CH11466, DE-FG02-08ER54999, DE-SC0019302 and DE-FC02-04ER54698.

REFERENCES

[1] ITER PHYSICS BASIS EDITORS, ITER Physics Expert Group Chairs and Co-Chairs, and ITER Joint Central Team and Physics Unit, Nucl. Fusion 39, (1999) 2137.
[2] MAINGI R., Enhanced confinement scenarios without large edge localized modes in tokamaks: control, performance, and extrapolability issues for ITER, Nucl. Fusion 54, (2014) 114016.
[3] Kotschenreuther, M. et al., Gyrokinetic analysis and simulation of pedestals to identify the culprits for energy losses using 'fingerprints', Nucl. Fusion 59 (2019) 096001.
[4] SAARELMA S., et al, MHD and gyro-kinetic stability of JET pedestals, Nucl. Fusion 53, (2013) 123012
[5] SNYDER P.B., et al., A first-principles predictive model of the pedestal height and width: development, testing and ITER optimization with the EPED model, Nuclear Fusion 51, (2011) 103016.
[6] VIEZZER E., et al., Investigation of inter-ELM ion heat transport in the H-mode pedestal of ASDEX Upgrade plasmas Nucl. Fusion 57, (2017) 022020.
[7] HASKEY S., et al., Main-ion Thermal Transport in High Performance DIII-D Edge Transport Barriers, APS-DPP invited talk, 2020
[8] HASKEY S., et al., Main-ion thermal transport in high performance DIII-D edge transport barriers, IAEA FEC 2020
[9] Conference proceedings
[10] CHEN J., et al., Pedestal magnetic turbulence measurements in ELMy H-mode DIII-D plasmas by Faraday-effect polarimetry, Physics of Plasmas 28, (2021) 022506.
[11] CHEN J., et al., Pedestal magnetic turbulence measurements in ELMy H-mode plasmas in DIII-D tokamak, IAEA FEC 2020 Conference proceedings
[12] GUTTENFELDER W., et al., Testing predictions of electron scale turbulent pedestal transport in two DIII-D ELMy H-modes, accepted manuscript Nuclear Fusion (2021)
[13] ASHOURVAN A., et al., Formation of a high pressure staircase pedestal with suppressed edge localized modes in the DIII-D tokamak, Phys. Rev. Lett. 123, (2019) 115001
[14] GROEBNER R. J. AND OSBORNE T. H., Scaling studies of the high mode pedestal, Phys. Plasmas 5, (1998) 1800.
[15] PEEBLES, W. A. et al, A novel, multichannel, comb-frequency Doppler backscatter system, Rev. Sci. Instrum. 81, (2010) 10D902.
[16] SMIRNOV, A. P. et al., in Proceedings of the 15th Workshop on ECE and ECRH (World Scientific, Singapore, 2009), p. 301; also see www.compxco.com/genray.html.
[17] DIALLO, A., et al., Correlations between quasi-coherent fluctuations and the pedestal evolution during the inter-edge localized modes phase on DIII-D, Physics of Plasmas 22, (2015) 056111
[18] DOYLE, E. J. et al., Chapter 2: Plasma confinement and transport, Nucl. Fusion 47 (2007): S18-S127.
[19] CASATI, A., et al, Temperature ratio dependence of ion temperature gradient and trapped electron mode instability thresholds, Phys. Plasmas, 15, (2008) 042310.
[20] STAEBLER, G. M. et al, A theory-based transport model with comprehensive physics. Physics of Plasmas 14 (2007) 055909.
[21] [20] BRESLAU J., GORELENKOVA M., POLI F., SACHDEV J. AND YUAN X., "TRANSP", Computer Software (2018)
[22] [21] BELLI E.A. AND CANDY J., Kinetic calculation of neoclassical transport including self-consistent electron and impurity dynamics, Plasma Physics and Controlled Fusion, 50, 095010 (2008)